Vol 16 No 12, December 2007
1009-1963/2007/16(12)/3719-09
Chinese Physics
© 2007 Chin. Phys. Soc.
and IOP Publishing Ltd

All-optical XNOR and AND gates simultaneously realized in a single semiconductor optical amplifier with improved dynamics*

Li Pei-Li(李培丽)[a)b)†], Huang De-Xiu(黄德修)[a)],
Zhang Xin-Liang(张新亮)[a)], and Zhu Guang-Xi(朱光喜)[a)b)]

[a)] *Wuhan National Laboratory for Optoelectronics, Huazhong University of Science and Technology, Wuhan* 430074, *China*
[b)] *Department of Electronics and Information, Huazhong University of Science and Technology, Wuhan* 430074, *China*

(Received 5 March 2007; revised manuscript received 20 April 2007)

All-optical XNOR and AND logic gates using four-wave mixing (FWM) and cross-gain modulation (XGM) in a single semiconductor optical amplifier (SOA) with improved dynamics are simultaneously realized. By numerical simulation, the effects of the input optical wave powers and injection current on the critical factors of the logic gate performances, such as the ON–OFF contrast ratio, the power-output level of the logic '1', and the difference between power outputs of the logic '1', are investigated in detail. In addition, the effect of the counter-propagating CW pump on the gain recovery is analysed.

Keywords: All-optical logic gate, four-wave mixing, cross-gain modulation, semiconductor optical amplifier

PACC: 4280S, 4280V

1. Introduction

All-optical signal processing would be widely applied in future high-speed optical networks. All-optical logic gates are crucial elements in all-optical signal processing which can realize all-optical demultiplexing, switching, buffering, and regenerating, etc. Many approaches to achieving all-optical logic functions, based on the nonlinear effects in semiconductor material, in optical fibres or in waveguides, have been proposed. In particular, all-optical logic gates based on the nonlinear effects in semiconductor optical amplifiers (SOAs), such as cross-gain modulation (XGM), cross-phase modulation (XPM), four-wave mixing (FWM), and cross-polarization modulation, are promising due to SOAs' high gain in the optical power, strong change of the refractive index and potential for photonic integration.

The XNOR and AND gates are the fundamental logic gates. All-optical XNOR gates have been demonstrated previously using two semiconductor micro-ring resonators,[1] an SOA based on a Mach–Zehnder interferometer,[2] and bacteriorhodopsin (bR) film[3] separately. Proposals for all-optical AND gates include using FWM in an SOA,[4] a semiconductor fibre ring laser[5] or semiconductor micro-ring resonators,[6] and using XGM in SOA[7,8] separately.

In this paper, all-optical XNOR and AND logic gates are simultaneously realized using the experimental scheme proposed in Ref.[9], in which simultaneous FWM and XGM in a single semiconductor optical amplifier are used. It should be noted that, different from being ignored in Ref.[9], the satellite wave and the conjugate wave both are used to realize the XNOR and AND logic gates simultaneously. So this scheme may potentially be used as an all-optical half-adder since it generates the AND and XNOR outputs simultaneously, which correspond to the CARRY and inverted-SUM outputs of a half adder.

The ON–OFF contrast ratio is a critical parameter for evaluating the logic gate performance, and in the general case of arbitrary input power levels, it can be defined as the ratio of average power-output of the logic '1' to the average power-output of the logic '0'

*Project supported by the National Natural Science Foundation of China (Grant No 60407001) and the National Science Foundation for Post-doctoral Scientists of China (Grant No 20060390246).
†E-mail: lplthl@sohu.com

in the output waveform. In addition to the ON–OFF contrast ratio, the power-output level of the logic '1' and the difference between power outputs of the logic '1' are also two important parameters of the logic gate performances. These parameters of the logic gate are chiefly dependent on the operating conditions, such as the powers of two input signals, probe and pump waves and the injection current. So the optimization of these operating conditions is essential for a low bit-error rate operation of the logic gate. In this paper, the effects of the input signals, probe and pump powers, injection current on the ON–OFF contrast ratio, the power-output level of the logic '1' and the difference between power outputs of the logic '1' are investigated in detail by numerical simulation. Also, the effect of the counter-propagating CW pump on the gain recovery is analysed.

2. Theory

The schematic diagram of all-optical XNOR and AND gates of this kind is shown in Fig.1(a). Two high-power signals at λ_1 and λ_2, combined with a low-power probe wave at λ_p, are injected into the SOA. Two input signals have the same polarizations. In the

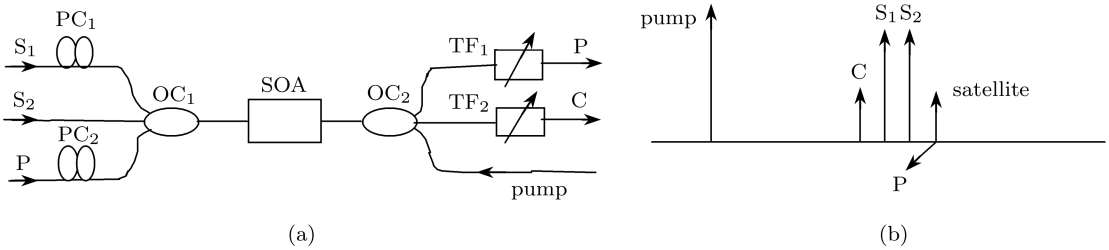


Fig.1. The schematic view of (a) all-optical XNOR and AND gates based on a single SOA with improved dynamics, and (b) the output optical spectra.

SOA, the FWM process occurs between two high-power signals and generates two new product waves, the conjugate and the satellite waves at $\lambda_c = 2\lambda_1 - \lambda_2$ and $\lambda_{sat} = 2\lambda_2 - \lambda_1$. The product waves have a pulse only when pulses are present in both of the input signals simultaneously. This corresponds to the AND operation. Since the two input signals both are strong and their wavelength interval is small, the generated FWM satellite wave is almost as strong as the conjugate wave. So the conjugate and the satellite waves both can realize the AND logic function. At the same time, the XGM process also occurs in the SOA. Each of the input signals acts as a pump wave for the XGM. Whenever a pulse is present in either of the input signals, the SOA's gain saturates and as a result the corresponding pulse at λ_p experiences a reduced gain while travelling through the SOA. Only those pulses are present at λ_p when both corresponding pulses at λ_1 and λ_2 are absent. This is equivalent to an NOR operation between the input signals. The XNOR logic corresponds to an OR operation between the AND and the NOR outputs. If the wavelength of probe wave is set to be equal to that of the satellite wave ($\lambda_{probe} = \lambda_{sat}$), the NOR output at λ_p and the AND output at λ_{sat} can be filtered simultaneously by centring the tunable filter 1 (TF_1) at λ_p, namely the XNOR function is achieved. So the XNOR and AND logic gates can be realized simultaneously by tuning TF_1 and TF_2 to filter the probe wave and the conjugate wave respectively. The corresponding truth table is shown in Table 1. To avoid phase interference between probe and FWM components, the polarization of input probe wave is orthogonal with those of the input signals. Also a counter-propagating continuous wave (CW) pump is introduced to improve the dynamic behaviour of the SOA. Furthermore, the CW pump wave can make the peak power outputs of probe and satellite waves equal approximately by reducing the gain of the probe wave, thus helping to realize the XNOR function effectively in this scheme.

Table 1. Corresponding truth table.

S_1	S_2	C(AND)	Sat(AND)	P (NOR)	P+Sat (XNOR)
0	0	0	0	1	1
0	1	0	0	0	0
1	0	0	0	0	0
1	1	1	1	0	1

In this scheme, due to the strong input signals and their small wavelength interval, the generated FWM satellite wave is almost as strong as the conjugate wave. So the satellite wave cannot be ignored. The FWM processes between the pump wave and the other waves are neglected because the pump is far from the other waves relatively. In our simulations, SOA is divided into n subsections along the longitudinal direction. When n is sufficiently large, the carrier density in each subsection is considered to be uniform. The travelling wave equations of the probe, signals, conjugate wave, satellite wave, and pump in subsection i can be expressed respectively as[10,11]

$$\frac{\mathrm{d}A_{\mathrm{p},i}}{\mathrm{d}z} = \frac{1}{2}\left[\frac{\Gamma g_{\mathrm{p},i}}{1+P_i/P_{\mathrm{s}}}(1-\mathrm{i}\alpha)-a_l\right]A_{\mathrm{p},i}, \tag{1}$$

$$\frac{\mathrm{d}A_{\mathrm{s1},i}}{\mathrm{d}z} = \frac{1}{2}\left[\frac{\Gamma g_{\mathrm{s1},i}}{1+P_i/P_{\mathrm{s}}}(1-\mathrm{i}\alpha)-a_l\right]A_{\mathrm{s1},i}-\frac{\Gamma g_{\mathrm{s1},i}}{2\left(1+P_i/P_{\mathrm{s}}\right)}\left(\eta_{\mathrm{s1,s2}}\left|A_{\mathrm{s2},i}\right|^2+\eta_{\mathrm{s1,c}}\left|A_{\mathrm{c},i}\right|^2+\eta_{\mathrm{s1,sat}}\left|A_{\mathrm{sat},i}\right|^2\right)$$
$$\times A_{\mathrm{s1},i}-\frac{\Gamma g_{\mathrm{s1},i}}{2\left(1+P_i/P_{\mathrm{s}}\right)}\left[\left(\eta_{\mathrm{s2,s1}}+\eta_{\mathrm{c,s1}}\right)A_{\mathrm{s2},i}A_{\mathrm{c},i}A^*_{\mathrm{s1},i}+\eta_{\mathrm{s2,sat}}A^2_{\mathrm{s2},i}A^*_{\mathrm{sat},i}\right], \tag{2}$$

$$\frac{\mathrm{d}A_{\mathrm{s2},i}}{\mathrm{d}z} = \frac{1}{2}\left[\frac{\Gamma g_{\mathrm{s2},i}}{1+P_i/P_{\mathrm{s}}}(1-\mathrm{i}\alpha)-a_l\right]A_{\mathrm{s2},i}-\frac{\Gamma g_{\mathrm{s2},i}}{2\left(1+P_i/P_{\mathrm{s}}\right)}\left(\eta_{\mathrm{s2,s1}}\left|A_{\mathrm{s1},i}\right|^2+\eta_{\mathrm{s2,c}}\left|A_{\mathrm{c},i}\right|^2+\eta_{\mathrm{s2,sat}}\left|A_{\mathrm{sat},i}\right|^2\right)$$
$$\times A_{\mathrm{s2},i}-\frac{\Gamma g_{\mathrm{s2},i}}{2\left(1+P_i/P_{\mathrm{s}}\right)}\left[\left(\eta_{\mathrm{s1,s2}}+\eta_{\mathrm{sat,s2}}\right)A_{\mathrm{s1},i}A_{\mathrm{sat},i}A^*_{\mathrm{s2},i}+\eta_{\mathrm{s1,c}}A^2_{\mathrm{s1},i}A^*_{\mathrm{c},i}\right], \tag{3}$$

$$\frac{\mathrm{d}A_{\mathrm{c},i}}{\mathrm{d}z} = \frac{1}{2}\left[\frac{\Gamma g_{\mathrm{c},i}}{1+P_i/P_{\mathrm{s}}}(1-\mathrm{i}\alpha)-a_l\right]A_{\mathrm{c},i}-\frac{\Gamma g_{\mathrm{c},i}}{2\left(1+P_i/P_{\mathrm{s}}\right)}\Big[\left(\eta_{\mathrm{c,s1}}\left|A_{\mathrm{s1},i}\right|^2+\eta_{\mathrm{c,s2}}\left|A_{\mathrm{s2},i}\right|^2+\eta_{\mathrm{c,sat}}\left|A_{\mathrm{sat},i}\right|^2\right)$$
$$\times A_{\mathrm{c},i}\Big],-\frac{\Gamma g_{\mathrm{c},i}}{2\left(1+P_i/P_{\mathrm{s}}\right)}\left[\left(\eta_{\mathrm{s2,sat}}+\eta_{\mathrm{s1,sat}}\right)A_{\mathrm{s1},i}A_{\mathrm{s2},i}A^*_{\mathrm{sat},i}+\eta_{\mathrm{s1,s2}}A^2_{\mathrm{s1},i}A^*_{\mathrm{s2},i}\right], \tag{4}$$

$$\frac{\mathrm{d}A_{\mathrm{sat},i}}{\mathrm{d}z} = \frac{1}{2}\left[\frac{\Gamma g_{\mathrm{sat},i}}{1+P_i/P_{\mathrm{s}}}(1-\mathrm{i}\alpha)-a_l\right]A_{\mathrm{sat},i}-\frac{\Gamma g_{\mathrm{sat},i}}{2\left(1+P_i/P_{\mathrm{s}}\right)}\left(\eta_{\mathrm{sat,s1}}\left|A_{\mathrm{s1},i}\right|^2+\eta_{\mathrm{sat,s2}}\left|A_{\mathrm{s2},i}\right|^2+\eta_{\mathrm{sat,c}}\left|A_{\mathrm{c},i}\right|^2\right)$$
$$\times A_{\mathrm{sat},i}-\frac{\Gamma g_{\mathrm{sat},i}}{2\left(1+P_i/P_{\mathrm{s}}\right)}\left[\left(\eta_{\mathrm{s2,c}}+\eta_{\mathrm{s1,c}}\right)A_{\mathrm{s1},i}A_{\mathrm{s2},i}A^*_{\mathrm{c},i}+\eta_{\mathrm{s2,s1}}A^2_{\mathrm{s2},i}A^*_{\mathrm{s1},i}\right], \tag{5}$$

$$\frac{\mathrm{d}A_{\mathrm{pump},i}}{\mathrm{d}z} = \frac{1}{2}\left[\frac{\Gamma g_{\mathrm{pump},i}}{1+P_i/P_{\mathrm{s}}}(1-\mathrm{i}\alpha)-a_l\right]A_{\mathrm{pump},i}, \tag{6}$$

where A is the normalized slowly varying envelope of the light field, $P_i=\sum_j\left|A_{j,i}\right|^2$ is the total optical power inside ith subsection, Γ is the mode confinement factor, $g_{j,i}(N)$ is the material gain coefficient of the SOA, P_{s} is the saturation power, α is the linewidth enhancement factor, and a_l is the loss of SOA. The coefficients $\eta_{jj'}$, $j\neq j'$, $j=\mathrm{s}_1,\mathrm{s}_2,\mathrm{c},\mathrm{sat}$ represent the nonlinear interactions among the mixing waves, and their expressions are given in Ref.[11]. The saturation power P_{s} is determined by

$$P_{\mathrm{s}}=\frac{h\nu wd}{\Gamma\tau_{\mathrm{e}}\mathrm{d}g/\mathrm{d}N} \tag{7}$$

where τ_{e} is the effective carrier lifetime and can be expressed as[12]

$$\frac{1}{\tau_{\mathrm{e}}}=\frac{1}{\tau_{\mathrm{s}}}+\sum_j\frac{g_{j,i}\cdot l+1}{g_{j,i}\cdot l}\cdot\frac{\mathrm{d}g_{j,i}}{\mathrm{d}N}\cdot\left|A_{j,i}\right|^2. \tag{8}$$

As indicated in expression (8), the injection of a CW pump wave reduces τ_{e}, namely, speeds up the gain recovery process. From expression (7) it is known that P_{s} is in inverse proportion to τ_{e}. Therefore, the injection of a pump wave increases P_{s}, which in turn raises the conversion efficiency of FWM effect.[13]

The material gain coefficient of the SOA $g_{j,i}(N)$ can be expressed as[14]

$$g(\nu,N)=\frac{e^2\left|M\right|^2}{4\pi^2\varepsilon_0m_0^2cn_{\mathrm{g}}\nu}\left(\frac{8\pi^2m_{\mathrm{c}}m_{\mathrm{hh}}}{h^2(m_{\mathrm{c}}+m_{\mathrm{hh}})}\right)^{3/2}$$
$$\times\left(h\nu-E_{\mathrm{g}}\right)^{1/2}\left[f_{\mathrm{c}}(\nu)+f_v(\nu)-1\right], \tag{9}$$

where N is the carrier density, e is the electron charge, h is Planck constant, ε_0 is the vacuum permittivity, m_0 is the free-electron mass, m_{c} is the conduction-band (CB) electron mass, m_{hh} is the effective mass of a heavy hole in the valence band (VB), c is the speed of light in vacuum, n_{g} is the refractive index, Δ is the spin-orbit splitting, $\left|M\right|^2$ is the momentum-matrix el-

ement, E_g is the band-gap energy, $f_c(\nu)$ and $f_v(\nu)$ are the Fermi-Dirac distributions for the conduction and valence bands, respectively:

$$f_c(\nu) = \frac{1}{\exp[(E_c - E_{fc})/k_B T] + 1}$$

and

$$f_v(\nu) = \frac{1}{\exp[(E_v - E_{fv})/k_B T] + 1}, \tag{10}$$

where E_c and E_v being

$$\begin{aligned} E_c &= \frac{m_r}{m_c}(h\nu - E_g), \\ E_v &= \frac{m_r}{m_{hh}}(h\nu - E_g), \\ m_r &= \frac{m_c m_{hh}}{m_c + m_{hh}}, \end{aligned} \tag{11}$$

and T being absolute temperature and k_B being the Boltzmann constant. E_{fc} and E_{fv} are the quasi-Fermi level of the CB relative to the bottom of the band and the quasi-Fermi level of the VB relative to the top of the band respectively. Their expressions are given in Ref.[14].

To calculate the amplified spontaneous emission (ASE) spectrum, the whole spontaneous emission spectrum is divided into m segments. The travelling wave equations for the ASE spectrum in the wavelength between λ_{j-1} and λ_j can be expressed as[16]

$$\begin{aligned} \pm\frac{dW^{\pm}_{j,i}(z,t)}{dz} &= [\Gamma g_{j,i}(N) - \alpha_l] W^{\pm}_{j,i}(z,t) \\ &\quad + \Gamma g'_{j,i} \frac{hc^2}{\lambda_j^3}, \end{aligned} \tag{12}$$

where $W_{j,i}(z,t)$ is the power spectrum density, and $g'_{j,i}$ is the stimulated emission rate per unit length of the SOA and is given by

$$\begin{aligned} g'(\nu, N) &= \frac{e^2 |M|^2}{4\pi^2 \varepsilon_0 m_0^2 c n_a \nu} \left(\frac{8\pi^2 m_r}{h^2}\right)^{3/2} \\ &\quad \times (h\nu - E_g)^{1/2} f_c(\nu) f_v(\nu). \end{aligned} \tag{13}$$

The carrier density in subsection i can be described by the rate equation

$$\begin{aligned} \frac{dN_i}{dt} &= \frac{I}{ewdL} - \left(c_1 N_i + c_2 N_i^2 + c_3 N_i^3\right) - \sum_{j=p,s_1,s_2,c,sat,pump} g_{j,i} \frac{G_{j,i} - 1}{\ln G_{j,i}} \frac{|A_{j,i}|^2 \lambda_j}{hcwd} \\ &\quad - \sum_{j=1}^{m} g_{j,i} \left[\frac{2 g_{j,i}}{\bar{g}_{j,i}} \left(\frac{G_{j,i} - 1}{\ln G_{j,i}} - 1 \right) + \frac{G_{j,i} - 1}{\ln G_{j,i}} \frac{\Delta\lambda \left(W^{+}_{j,i} + W^{-}_{j,i}\right) \lambda_j}{hcwd} \right], \end{aligned} \tag{14}$$

where I is the injection current, wdL is the volume of the active region, c_1 is the Nonradiative recombination coefficient, c_2 is the bimolecular recombination coefficient, c_3 Auger recombination coefficient, and $G_{j,i} = \exp(\bar{g}_{j,i} \Delta l)$ is the gain of subsection i. The third and fourth terms on the right-hand side of Eq.(14) are the carrier consumption induced by the stimulated emission for the signal, conjugate wave, pump wave, probe wave, and the ASE.

3. Simulation results and discussion

The parameters used in our simulation are listed in Table 2.

In the simulations, the return-to-zero (RZ) bit sequences have been used for two signals at 40 Gb/s with 5 ps-wide pulses. The peak powers of two input signals are both 12 dBm. The probe is a pulsed clock, synchronized with two input signals, with a peak power of −15 dBm. Here, the low-power levels are all set to be 0 mW. The CW pump power is 1 dBm. The wavelengths for the two input signals, probe and pump waves are 1550, 1551, 1552 and 1540 nm, respectively. Thus the wavelengths of the produce signals, conjugate and satellite waves, are 1549 and 1552 nm, respectively.

Figure 2 shows the simulation results of all-optical XNOR and AND logic gates of this kind. The bit sequences in Figs.2(a) and (b) are '0011000100' and '0001100100' for two input signals. The bit sequences in Figs.2(c) and (d) are '1101011111' for probe wave and '0001000100' for conjugate wave. They are just the XNOR and the AND between two input signals.

Table 2. Parameters used in simulation

Parameter	Symbol	Value
Length of active region	$L/10^{-3}$m	1
Width of active region	$w/10^{-6}$m	3.3
Thickness of active region	$d/10^{-6}$m	0.15
Nonradiative recombination coefficient	$c_1/10^{8}$s^{-1}	1.5
Bimolecular recombination coefficient	$c_2/10^{-17}$m^{3}s^{-1}	2.5
Auger recombination coefficient	$c_3/10^{-41}$m^{6}s^{-1}	9.4
Internal loss of SOA	$\alpha_l/10^{3}$m^{-1}	4
Optical confinement factor	Γ	0.3
Refractive index	$n_{\rm a}$	3.22
Linewidth enhancement factor by CH	$\alpha_{\rm CH}$	3.6
Linewidth enhancement factor by SHB	$\alpha_{\rm SHB}$	0.1
Carrier heating parameter	$\varepsilon_{\rm CH}$/W^{-1}	4
Spectral hole burning parameter	$\varepsilon_{\rm SHB}$/W^{-1}	6
Carrier lifetime	$\tau_{\rm s}/10^{-10}$ s	1.6
Spectral hole burning time	$\tau_2/10^{-13}$s	1.0
Carrier heating time	$\tau_1/10^{-13}$s	6.5
Effective mass of electron in the CB	$m_{\rm c}/10^{-32}$ kg	4.10
Effective mass of a heavy hole in the VB	$m_{\rm hh}/10^{-31}$ kg	4.19
Effective mass of electron in the CB	$m_{\rm lh}/10^{-32}$ kg	5.06
Coupler 1 coefficient	k_1	1:1:1
Coupler 2 coefficient	k_2	1:1:1
The beginning wavelength of ASE spectra	$\lambda_1/10^{-6}$m	1.500
The ending wavelength of ASE spectra	$\lambda_{\rm m}/10^{-6}$m	1.600

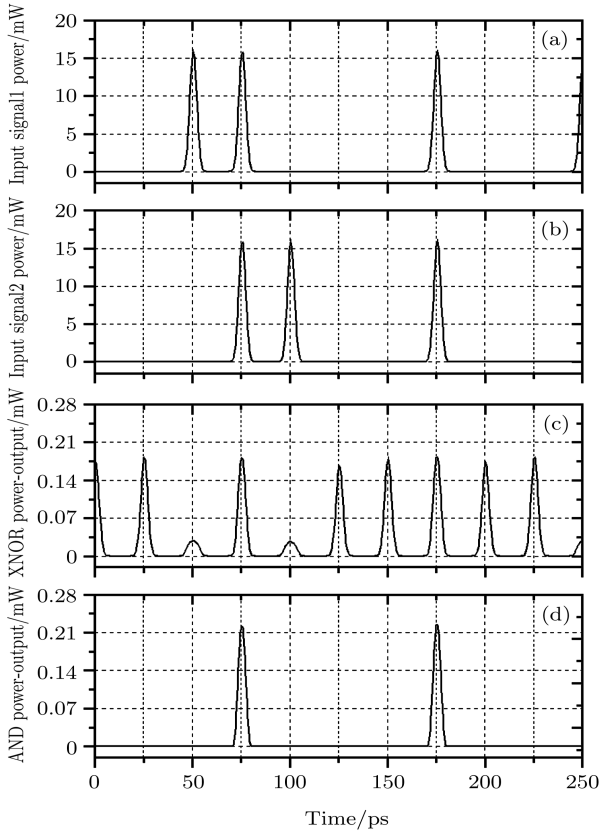


Fig.2. (a) The input sequence of signal 1, (b) the input sequence of signal 2, (c) the output sequence of the XNOR gate, and (d) the output sequence of the AND gate.

Also, it can be seen from Fig.2(c) that some small pulses are present at the '0' level of the XNOR logic output, as can be found in Ref.[7]. The reason for that is that the peak powers of the two signals are not large enough to saturate the SOA deeply. Although it can be eliminated by increasing the peak power of signals, the peak power-output of satellite wave would be larger than that of the probe wave. The XNOR logic is equivalent to coupling together the AND and NOR outputs. As a result, in this case the difference between power outputs of the XNOR logic '1' becomes larger and the XNOR output signal quality reduces.

As mentioned earlier, the counter-propagating high-power CW pump can reduce the mean lifetime of the carriers. So the effect of the counter-propagating CW pump on the gain recovery is investigated. Figure 3 shows the gain recovery dynamics of the SOA with and without the pump wave of 1 dBm power. The peak powers of the signal and probe wave are 9 dBm and −8 dBm, respectively. It is clear that the gain recovery time of SOA is effectively reduced by the injected pump; however, the power output of probe wave becomes weak. It is also shown in Ref.[8]. This is because that the pump wave is in the gain region of SOA spectrum, thus inducing a large reduction in avail-

able gain. In this scheme, in addition to reducing the gain recovery time and making the scheme suitable for ultra-fast applications, the counter-propagating CW pump also makes the XNOR function realized effectively. It is well known that the conjugate and satellite waves generated by FWM process are weak, though the power output of probe wave is relatively strong.

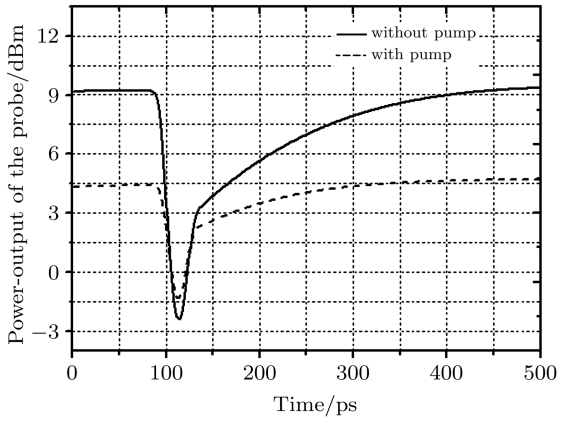


Fig.3. Gain recovery time of the SOA with and without the injection of the counter-propagating pump.

Therefore the difference between power outputs of the XNOR logic '1' is very large. This case cannot satisfy the logic gate's need, whereas the introduced pump wave, which is in the gain spectrum of SOA, can reduce the gain of the probe wave largely. Hence the peak power-outputs of probe and satellite waves can be equal approximately.

The performances of all-optical XNOR and AND gates of this kind with respect to the powers of the input optical waves are investigated in detail.

Figures 4(a) and (b) show, respectively, power-output sequences of all-optical logic XNOR and AND gates of this kind under $I = 250\,\mathrm{mA}$, $P_\mathrm{p} = -15\,\mathrm{dBm}$, and $P_\mathrm{pump} = 1\,\mathrm{dBm}$ for different input signal powers. Clearly, the peak power-outputs of the conjugate and satellite waves increase; however, the peak power-output of the probe wave decreases along with the peak powers of the input signals rising. The reason is that the larger input signals consume more carriers that would otherwise contribute to the probe wave. So, too a high or too a low input-signal power can increase the difference between power outputs of the XNOR logic '1'. From Fig.4(b) it can be seen that the AND '1' power-output increases as the peak powers of two signals rise.

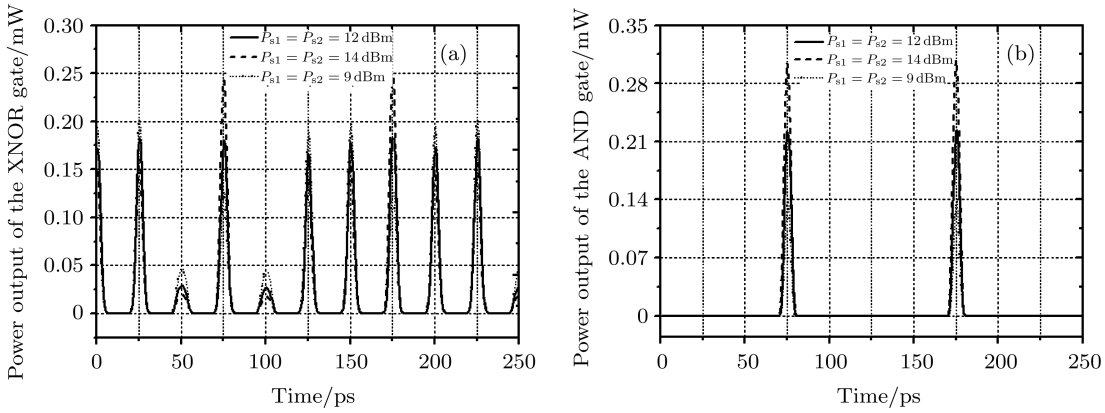


Fig.4. (a) The output sequence of the XNOR gate, and (b) the output sequence of the AND gate for different input-signal powers under $I = 250\,\mathrm{mA}$, $P_\mathrm{p} = -15\,\mathrm{dBm}$, and $P_\mathrm{pump} = 1\,\mathrm{dBm}$.

Figure 5 shows the effects of the input power of probe wave on the power outputs of the XNOR and the AND gates. Similar to the case of input-signal powers, too a large (too small) power of probe wave induces a large (small) power output of probe wave, thus resulting in the large difference between power outputs of the XNOR logic '1'. Since the input-signal powers are fixed, the AND outputs are almost equal as the input power of probe wave varies.

The difference between power outputs of the XNOR logic '1' would be very small by optimizing the input powers of two signals and probe wave, namely, the power of probe wave increases or decreases along with two signals increasing or decreasing respectively. Figure 6 shows the XNOR output sequences and the AND output sequences with the peak powers of input signals being 9, 12 and 14 dBm, the corresponding peak powers of input probe wave being −17.5, −15

and −13 dBm, respectively. Comparing Fig.3 with Fig.4, it can be seen clearly that the difference between power outputs of the XNOR logic '1' is small. Furthermore, stronger input optical waves not only result in a higher ON–OFF contrast ratio but also increase the XNOR and the AND power-output level of logic '1'.

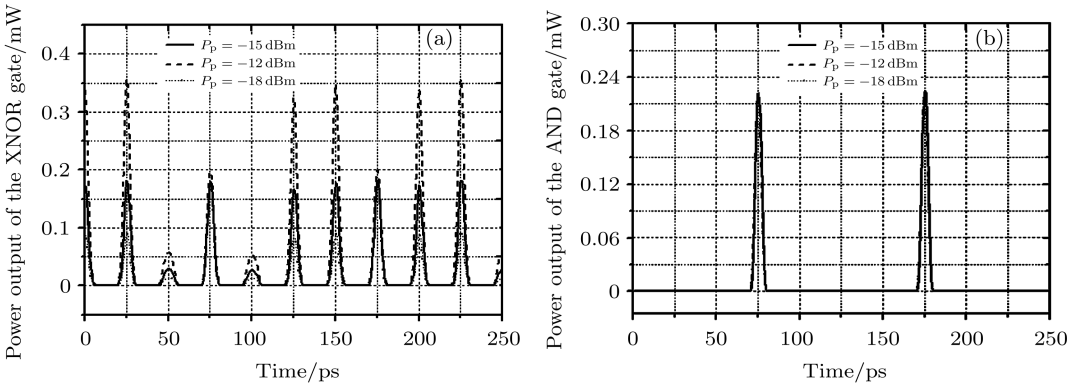


Fig.5. (a) The output sequence of the XNOR gate, and (b) the output sequence of the AND gate for different powers of input probe wave under $I = 250$ mA, $P_{s1} = P_{s2} = 12$ dBm, and $P_{pump} = 1$ dBm.

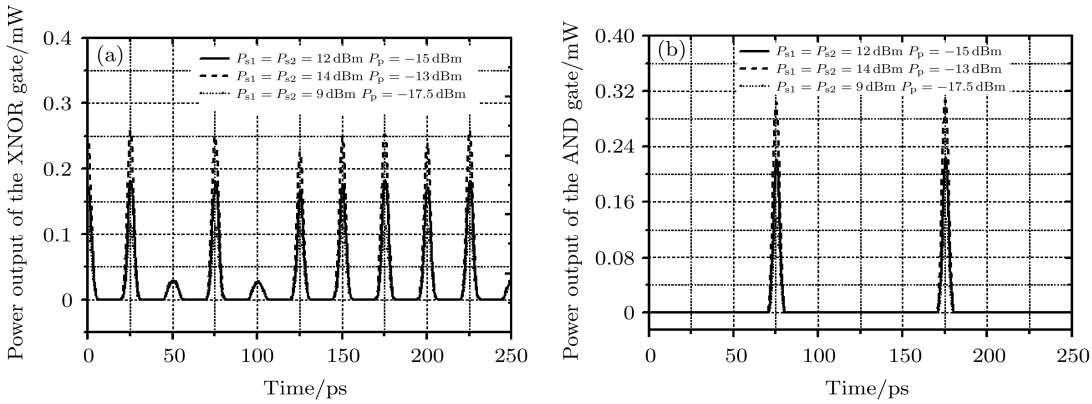


Fig.6. (a) The output sequence of the XNOR gate, and (b) the output sequence of the AND gate for different power optimization combinations of the signals and the probe under $I = 250$ mA, and $P_{pump} = 1$ dBm.

The effects of the input-pump power on the power outputs of the XNOR and the AND gates are also investigated. When the pump power increases, the gain recovery is sped up, as can be seen in Fig.7(a). It is in agreement with the foregoing analysis. Because a stronger pump wave induces a larger reduction in available gain, the power outputs of the XNOR and the AND decrease as the input-pump power increases. In the XNOR output sequence, it can also be seen that, corresponding to a stronger pump wave, the peak power-output of satellite wave is larger than that of the probe wave. This is attributed to the fact that, as analysed earlier, a smaller τ_e induces increasing P_s as well as FWM conversion efficiency. On the contrary, the peak power-output of satellite wave is smaller than that of the probe wave in the XNOR output sequence, corresponding to the case of weaker pump wave.

From Fig.7(a), we know that when the pump wave is too strong (too weak), the difference between power outputs of the XNOR logic '1' should be larger by weakening (strengthening) the input signals or strengthening (weakening) the input probe-wave. Figure 8 shows the XNOR sequences and the AND output sequences for different power optimization combinations of the pump wave and the signals under $P_{probe} = -15$ dBm and $I = 250$ mA. We can see from these cases that the difference between power outputs of the XNOR logic '1' becomes small. The ON–OFF contrast ratio and the power-output level of logic '1' are improved as the pump wave is weaker. However, the strong pump-wave speeds up the gain recovery rate and make the scheme suitable for ultrafast applications. By optimizing the input powers of pump wave and probe wave, the similar results can also be achieved.

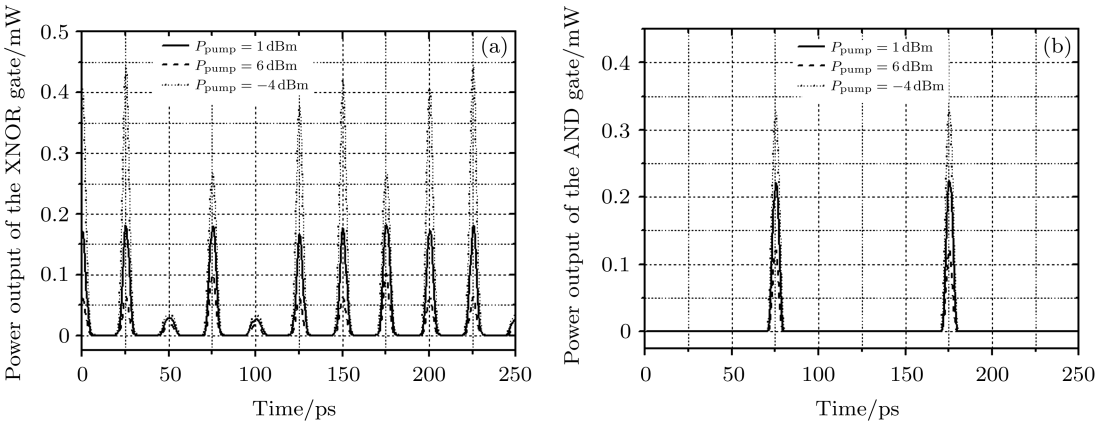


Fig.7. (a) The output sequence of the XNOR gate, and (b) the output sequence of the AND gate for different input-pump powers under $I = 250\,{\rm mA}$, $P_{\rm s1} = P_{\rm s2} = 12\,{\rm dBm}$, and $P_{\rm p} = -15\,{\rm dBm}$.

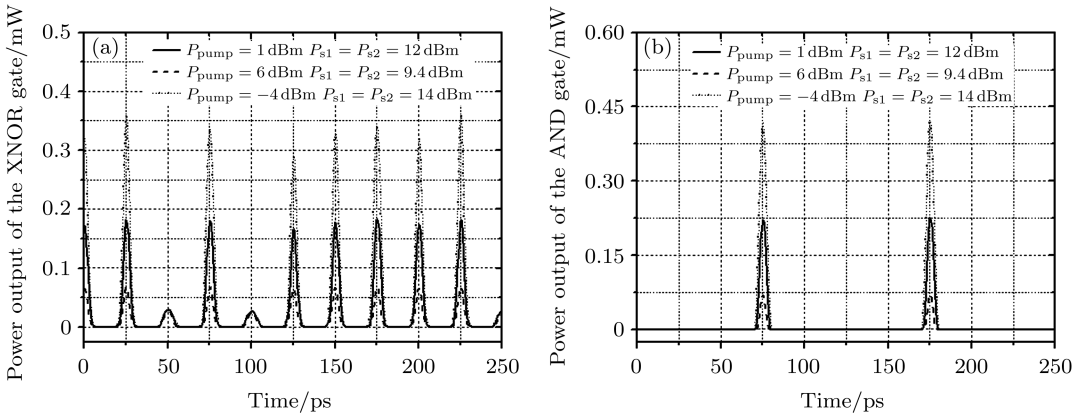


Fig.8. (a) The output sequence of the XNOR gate, and (b) the output sequence of the AND gate for different power optimization combinations of the pump and the signals under $I = 250\,{\rm mA}$, $P_{\rm s1} = P_{\rm s2} = 12\,{\rm dBm}$, and $P_{\rm p} = -15\,{\rm dBm}$.

Similar to a CW pump wave, the gain recovery rate can be moderately sped up by increasing the injected current. Figure 9 shows the XNOR output sequences and the AND output sequences for different injection currents. With the injection current rising, the carrier density as well as the available gain increase. As a result, the XNOR and the AND power-output level of logic '1' increase as the injection current rises. Moreover, the ON–OFF contrast ratio of XNOR output signal is improved too. However, in fact, the current cannot increase as much as desired because the heat generated due to high injection-current and the thermal-related degradation will limit the lever of the injection current that can be applied to the device.

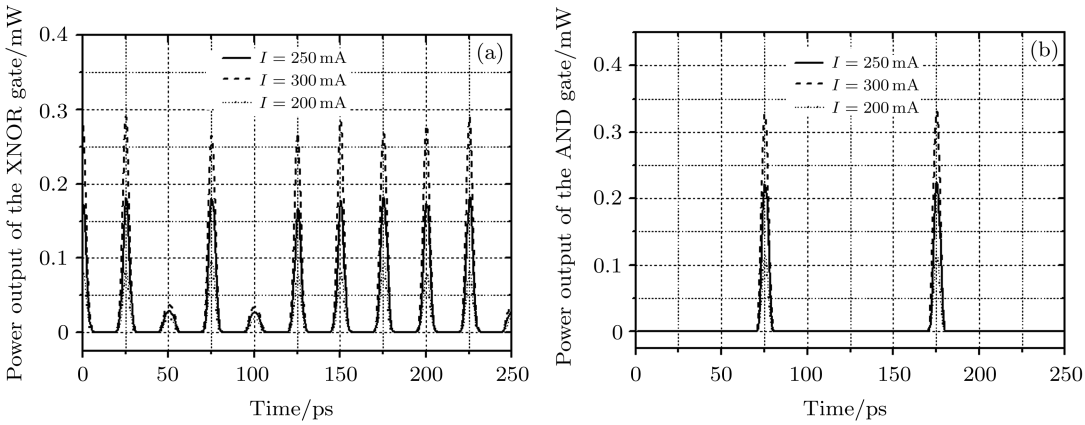


Fig.9. (a) The output sequence of the XNOR gate and (b) the output sequence of the AND gate for different injection currents under $P_{\rm s1} = P_{\rm s2} = 12\,{\rm dBm}$, $P_{\rm p} = -15\,{\rm dBm}$, and $P_{\rm pump} = 1\,{\rm dBm}$.

4. Conclusion

All-optical XNOR and AND logic gates using FWM and XGM in a single SOA with improved dynamics are simultaneously realized and investigated. It has been shown that in this scheme the powers of input optical waves should be optimized, otherwise the difference between power outputs of the XNOR logic '1' would be too large. For a certain power of the pump wave, the larger optimized powers of the signals and probe wave induce a higher ON–OFF contrast ratio and a larger power-output level of logic '1'. The introduced CW pump wave can reduce the gain recovery time. Moreover, it makes the peak power-outputs of probe and satellite waves equal approximately and help to realize the XNOR function effectively in this scheme. By optimizing the input signal powers or the input power of probe wave, the ON–OFF contrast ratio and the power-output level of logic '1' both can be improved as the power of the pump wave decreases. Also, the performances of all-optical XNOR and AND logic gates of this kind are improved by increasing the injection current.

References

[1] Van V, Ibrahim T A, Absil P P, Johnson F G, Grover R and Ho P T 2002 *IEEE J. Select. Topics Quantum Electron.* **8** 705

[2] Lee S, Park J, Lee K, Eom D, Lee S and Kim J 2002 *Japanese J. Appl. Phys.* **41** L1155

[3] Chen G Y, Zhang C P, Guo Z X, Tian J G, Zhang G Y and Song Q W 2005 *Chin. Phys.* **14** 774

[4] Nesset D, Tatham M C and Cotter D1995 *Electron. Lett.* **31** 896

[5] Li P L, Huang D X, Zhang X L and Zhu G X 2007 *Acta Phys. Sin.* **56** 871 (in Chinese)

[6] Mikroulis S, Simos H, Roditi E and Syvridis D 2005 *IEEE Photon Technol. Lett.* **17** 1878

[7] Zhang X L, Dong J J, Zhao C and Huang D X 2005 *Acta Phys. Sin.* **54** 2066 (in Chinese)

[8] Zhao C, Zhang X L, Dong J J and Huang D X 2006 *Acta Phys. Sin.* **55** 4150 (in Chinese)

[9] Berrettini G, Malacarne A, Ghelfi P, Bogoni A and Poti L 2006 *IEEE Photon Technol. Lett.* **18** 1341

[10] Kothari N C and Blumenthal D J 1996 *IEEE J. Quantum Electron.* **32** 1810

[11] Simos H, Bogris A and Syvridis D 2004 *IEEE J. Lightwave Technol.* **22** 595

[12] Hsieh J T, Gong P M, Lee S L and Wu J 2004 *IEEE J. Select. Topics Quantum Electron.* **10** 1187

[13] Ottavi A D, Girardin F, Graziani L, Martelli F, Spano P, Mecozzi A, Scotti S, Dall A R, Eckner J and Guekos G 1997 *IEEE J. Select. Topics Quantum Electron.* **3** 522

[14] Mikkelson B 1994 *Ph.D Thesis* (Denmark Technical University) 163

[15] Nilsson N G 1978 *Appl. Phys. Lett.* **33** 653

[16] Talli G and Adams M J 2003 *Optics Commun.* **218** 161